Sequence structure organizes items in varied latent states of working memory neural network

Qiaoli Huang[1-3], Huihui Zhang[1-3], Huan Luo[1-3, *]

[1] School of Psychological and Cognitive Sciences, Peking University

[2] PKU-IDG/McGovern Institute for Brain Research, Peking University

[3] Beijing Key Laboratory of Behavior and Mental Health, Peking University

Running title:

Backward reactivation for sequence memory

Address for Correspondence:

* Huan Luo

School of Psychological and Cognitive Sciences, Peking University

PKU-IDG/McGovern Institute for Brain Science, Peking University

Room 1703, 52 Haidian Road, Beijing, 100087, China

huan.luo@pku.edu.cn

Abstract

In memory experiences, events do not exist independently but are linked with each other via structure-based organization. Structure knowledge largely influences memory behavior, but how it is implemented in the brain remains unknown. Here, we combined magnetoencephalogram (MEG) recordings, computational modeling, and impulse-response approaches to probe the latent states when subjects held a list of items in working memory (WM). We demonstrate that sequence structure reorganizes WM items into distinct latent states, i.e., being reactivated at different latencies, and the reactivation profiles further correlate with recency behavior. In contrast, memorizing the same list of items without sequence requirements disrupts the recency effect and elicits comparable reactivations. Finally, computational modeling reveals a dominant function of high-level representations that characterize the abstract sequence structure, instead of low-level information decaying, in mediating sequence memory. Taken together, sequence structure shapes the way WM items are stored in the brain and essentially influences memory behavior.

Keywords: working memory; hidden state; backward reactivation, recency effect; sequence structure; Bayesian integration modeling

Introduction

Working memory (WM) refers to the brain system that could provide temporary storage and manipulation of information to guide future behavior (Baddeley, 2003). It has long been posited that WM depends on persistent neuronal firing (Curtis & D'Esposito, 2003; Goldman-Rakic, 1995), but recent computational modeling and neuroimaging studies suggest that the sustained activities might not be necessary and instead, information could be stored in "activity-silent' hidden states, via changes in synaptic weights of the WM network (Miller et al., 2018; Mongillo et al., 2008; Rose et al., 2016; Sprague et al., 2016; Stokes, 2015; Trübutschek et al., 2017; Wolff et al., 2017). Recently, an intriguing impulse-response approach has been developed to reactivate WM information retained in the activity-silent network (Rose et al., 2016; Wolff et al., 2017). Using this approach, it has been found that multiple WM items are stored in active or non-active states, according to top-down attention (Rose et al., 2016; Wolff et al., 2017, 2020).

In addition to the top-down rule in terms of attentional demands (i.e., more or less task-related), multiple items could also be organized based on abstract structures or high-level knowledge, which has been shown to guide and even modify our low-level sensory perception and memory (Ahissar & Hochstein, 2004; Bae et al., 2015; Brady & Alvarez, 2011; Chen, 1982; Ding et al., 2017; Navon, 1977). Here, we focused on sequence structure, a typical structure that widely occurs in many cognitive functions, e.g., sequence memory, speech, movement control, and its neural implementation in WM. Specifically, we examined the hypothesis that items of equal task relevance but located at different positions in a sequence might be stored in different latent states of the WM neural network. The hypothesis is also motivated by our previous findings showing a backward reactivation profile for sequence memory, implying a more excitable state for recent items vs. early items (Huang et al., 2018).

To this end, we recorded magnetoencephalography (MEG) signals when human subjects retained a sequence of orientations as well as their ordinal positions in WM. A time-resolved multivariate inverted encoding model (IEM) (Brouwer & Heeger, 2009, 2011; Sprague et al., 2014) was used to reconstruct the neural representations of each orientation in the sequence (i.e., 1st item, 2nd item), throughout the delay period. Importantly, an impulse stimulus was presented during retention, aiming to transiently

perturb the WM network and probe the latent states of the stored items. Our results demonstrate a backward reactivation profile such that the transient impulse triggers the neural representation of the 2nd item first, followed by that of the 1st item, supporting their associated different latent states. Moreover, the neural reactivation pattern well predicts the recency effect in subsequent WM behavior, on a subject-by-subject basis. In contrast, in another MEG experiment when subjects retained the same sequence without needing to memorize the ordinal structure, the two serially presented items show similar reactivation profiles and decreased recency effect. Finally, a two-stream Bayesian integration model and full-parameter simulations demonstrate that the high-level stream that conveys the sequence structure knowledge, instead of the low-level stream that signifies the passive memory decay, largely characterizes the recency effect in WM behavior and further correlates with neural reactivations. Our findings constitute converging behavioral, neural, and modeling evidence supporting a central function of abstract sequence structure in working memory via reorganizing information representations in the brain and influencing memory behavior.

Results

Experimental procedure and recency behavior (Experiment 1)

Twenty-four subjects participated in Experiment 1 and their brain activities were recorded using a 306-channel magnetoencephalography (MEG) system (Elekta Neuromag system, Helsinki, Finland). As shown in Figure 1A, each trial consists of three periods – encoding, maintaining, and recalling. During the encoding period, participants viewed two serially presented grating stimuli and were instructed to memorize the two orientations as well as their order (1st and 2nd orientations). After a 2 sec maintaining period, a retrospective cue (retro-cue) appeared to instruct subjects which item (1st or 2nd) would be tested. Next, a probe grating was presented and participants indicated whether the orientation of the probe was rotated clockwise or anticlockwise relative to that of the cued grating. Note that since the retro-cue appeared only during the recalling period, subjects would need to hold the two WM orientations simultaneously in WM throughout the retention interval. Critically, during the maintaining period, a high-luminance 'impulse' stimulus that does not contain any orientation information was presented, aiming to transiently perturb the WM network so that the stored information and its associated latent states could be assessed.

As shown in Figure 1B, the memory behavioral performance exhibited the typical recency effect, i.e., 2nd > 1st item (N = 24, 1st item: mean = 0.77, s.e. = 0.012; 2nd item: mean = 0.79, s.e = 0.013; paired t-test, df = 23, t = 2.18, p = 0.039, Cohen's d = 0.45), consistent with previous findings (e.g., Broadbent & Broadbent, 1981; Huang et al., 2018). When plotting the psychometric function of the proportion of clockwise response as a function of angular difference between the probe and the cued WM grating, the 2nd item showed steeper slope than the 1st item (Figure 1C; 1st item: mean = 0.11, s.e. = 0.009; 2nd item: mean = 0.14, s.e = 0.015; paired t-test, df = 23, t = 2.64, p = 0.015, Cohen's d = 0.54). This pattern could be reliably observed for individual subjects (Figure 1D), consistently supporting the recency effect.

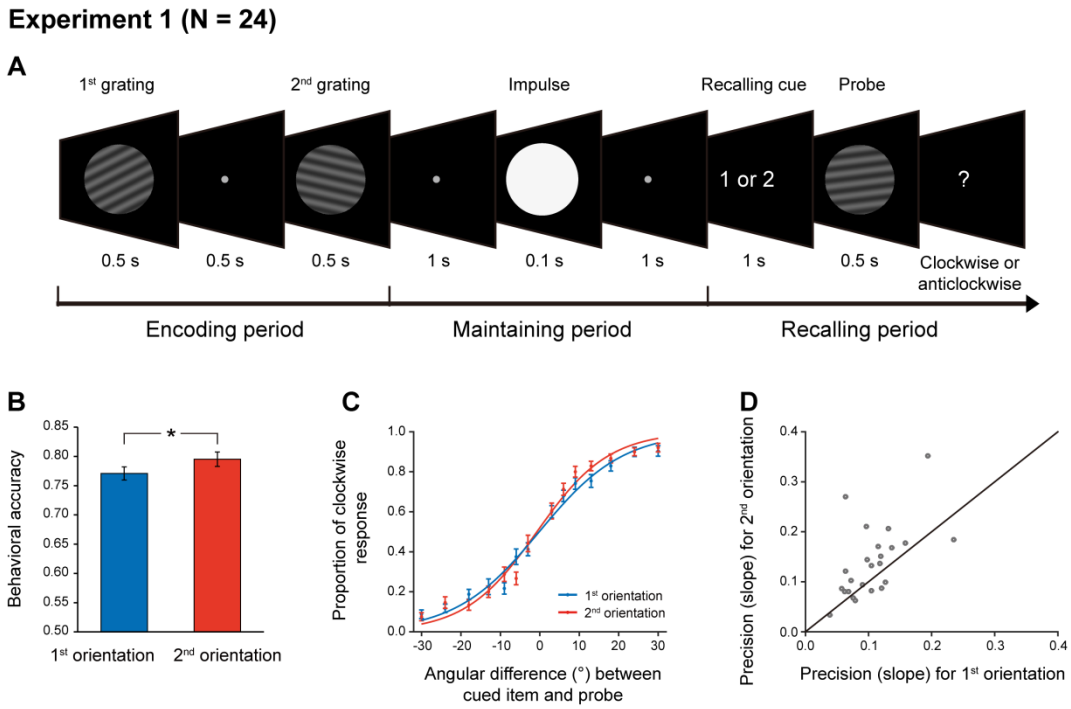

Figure 1: Experimental paradigm and recency effect (Experiment 1).
(A) Experiment 1 paradigm (N = 24). Subjects were first sequentially presented with two grating stimuli (1st and 2nd gratings) and needed to memorize the orientations of the two gratings as well as their temporal order (1st or 2nd orientation). During the maintaining period, a high luminance disc that does not contain any orientation information was presented as an impulse to disturb the WM neural network. During the recalling period, a retro-cue first appeared to instruct subjects which item (1st or 2nd) would be tested. Next, a probe grating was presented and participants indicated whether the orientation of the probe was rotated clockwise or anticlockwise relative to that of the cued grating. (B) Grand average (mean ± SEM) behavioral accuracy for the 1st (blue) and 2nd (red) orientations. (C) Grand average (mean ± SEM) psychometric functions for the 1st (blue) and 2nd (red) items as a function of the angular difference between the probe and cued orientation. Note the steeper slope for the 2nd vs. 1st orientation, i.e., recency effect. (D) Scatter plot for the slope of the psychometric function for the 1st (x axis) and 2nd orientations (y axis). (*: $p < 0.05$).

Time-resolved neural representations of orientation features (Experiment 1)

We used a time-resolved inverted encoding model (IEM) (Brouwer & Heeger, 2009, 2011; Sprague et al., 2014) to reconstruct the neural representations of orientation features at each time point throughout the experimental trial. We first verified this method by applying it to the encoding period when the to-be-memorized grating stimuli were presented physically. Specifically, the orientation decoding performance was characterized by a tuning curve as a function of angular difference between an orientation-of-interest and other orientations (see details in Methods). If MEG signals do carry information about specific orientation, the tuning curve would reveal a peak at center and gradually decrease on both sides. Figure 2AB plot the tuning curves for

the 1st and 2nd WM orientations, respectively, as a function of time throughout the encoding phase. It is clear that right after the presentation of the 1st grating, the tuning curve for the 1st orientation showed central peak (Figure 2A), whereas the tuning curve for the 2nd orientation displayed information representation only after the presentation of the 2nd grating (Figure 2B). To further quantify the time-resolved decoding performance, the slope of the tuning curve was estimated at each time point in each trial, for the 1st and 2nd orientations, respectively (see details in Methods). As shown in Figure 2C, the 1st orientation (blue) showed information representation right after the 1st grating (0.05 – 0.39 s, corrected cluster $p = 0.002$; 0.5 – 0.88 s, corrected cluster $p < 0.001$; 1.13 – 1.4 s, corrected cluster $p = 0.002$), and neural representation of the 2nd orientation (red) emerged after the 2nd grating (1.06 – 1.5 s, corrected cluster $p < 0.001$; 1.57 – 1.86 s, corrected cluster $p = 0.008$). Therefore, orientation information could be successfully decoded from MEG signals in a time-resolved manner. Moreover, the decoding performance for both the 1st and 2nd orientations gradually decayed to baseline, around 0.5 s after the offset of the 2nd item, suggesting that the WM network now entered the activity-silent WM states (Rose et al., 2016; Stokes, 2015; Wolff et al., 2017).

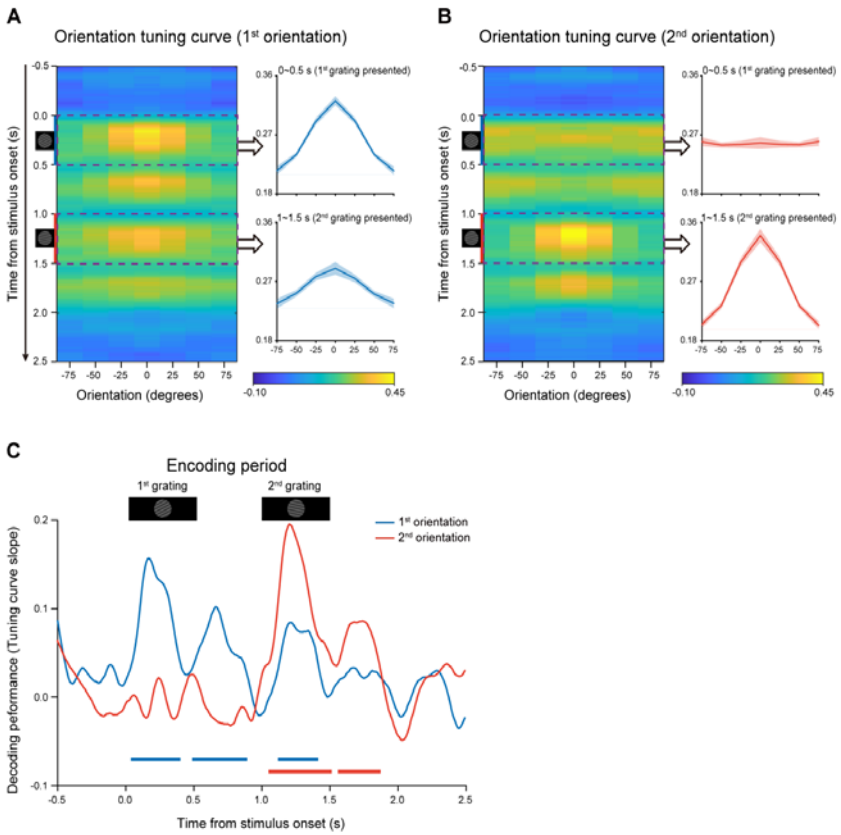

Figure 2: Time-resolved orientation representations during encoding period (Experiment 1). An IEM was used to reconstruct the neural representation of orientation features, characterized as a population tuning curve as a function of angular difference between particular orientation and other orientations (x-axis) at each time bin (y-axis). Successful encoding of orientation features would show a peak at center around 0 and gradually decrease on both sides, whereas lack of orientation information would have a flat tuning curve. The slope of the tuning curve was further calculated (see methods for details) to index information representation. (A) Left: Grand average time-resolved tuning curve for the 1st orientation (orientation of the 1st WM grating) throughout the encoding period during which the 1st and 2nd gratings (small inset figures on the left) were presented sequentially. Right: grand average (mean ± SEM) tuning curve for the 1st orientation averaged over the 1st grating presentation period (0 – 0.5 s, upper) and the 2nd grating presentation (1 – 1.5 s, lower). (B) Left: Grand average time-resolved tuning curve for the 2nd orientation (orientation of the 2nd WM grating) during the encoding period. Right: grand average (mean ± SEM) tuning curve for the 2nd orientation averaged over the 1st (0 – 0.5 s, upper) and 2nd (1 – 1.5 s, lower) grating presentation period. (C) Grand average time courses of the tuning curve slopes for the 1st (blue) and 2nd (red) orientations during the encoding period. Horizontal lines below indicate significant time ranges (cluster-based permutation test, cluster-defining threshold $p < 0.05$, corrected significance level $p < 0.05$) for the 1st (blue) and 2nd (red) orientations.

Impulse elicits backward reactivations during retention (Experiment 1)

After confirming the decoding approach in the encoding period, we next used the same analysis to examine the orientation representations held in WM that would be presumably reactivated by the impulse stimulus during retention (see Figure 1A). Figure 3A plots the decoding performances for the 1st (blue) and 2nd (red) WM orientation features, as a function of time after the impulse stimulus. Interestingly, instead of being activated simultaneously, the 1st and 2nd orientations showed distinct temporal profiles, i.e., the 2nd orientation showed earlier activation (T1: from 0.26 to 0.43 s, corrected cluster $p = 0.011$) than the 1st orientation (T2: from 0.67 to 0.76 s, corrected cluster $p = 0.030$), with approximately 0.4 s temporal lag in-between. To further verify their distinct patterns, we computed the difference (Figure 3B) and sum (Figure 3C) between the 1st and 2nd decoding temporal profiles. The difference course was significant (0.31 – 0.42 s, corrected cluster $p = 0.023$; 0.62 – 0.75 s, corrected cluster $p = 0.013$) (Figure 3B), while their sum did not show any significance (Figure 3C), further confirming that the two items were activated at different latencies. The results suggest that the 1st and 2nd items, instead of residing in equally excitable hidden states, tend to be stored in different latent states of the WM network. As a consequence, a transient perturbation of the network would produce an early 2nd item reactivation and a late 1st item response.

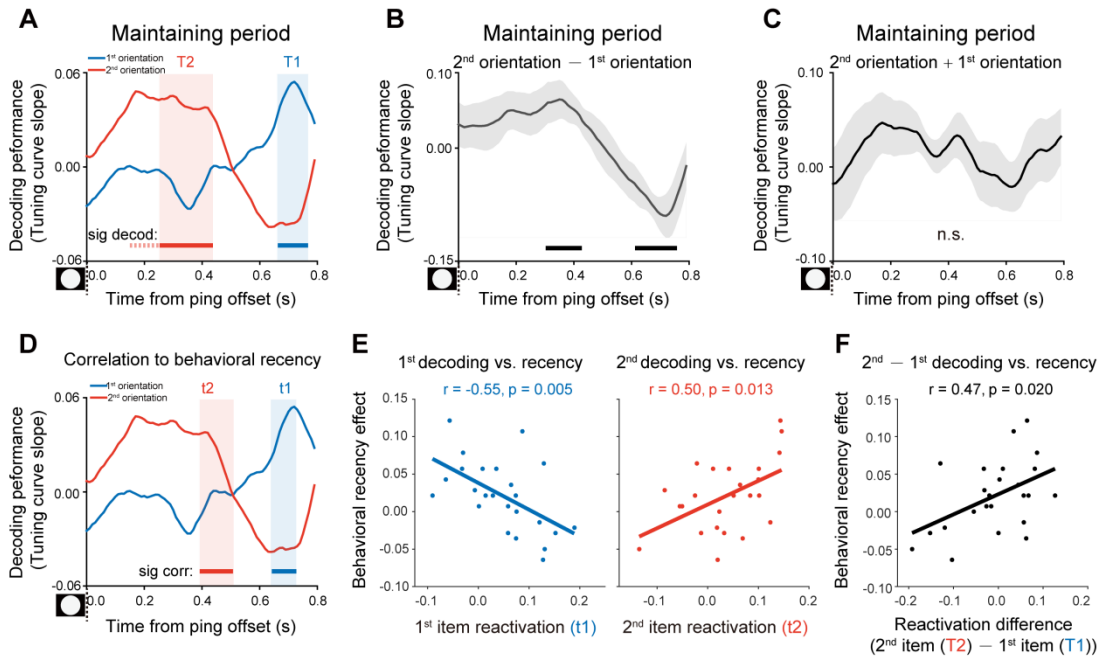

Figure 3: Backward reactivations during retention and behavioral relevance (Experiment 1). (A) Grand average time courses of the tuning curve slope for the 1st (blue) and 2nd (red) WM orientations after the impulse (inset in the bottom left) during the delay period. Horizontal lines below indicate time ranges of significant decoding strengths for the 1st (blue, T1) and 2nd (red, T2) orientations, respectively. (B) Grand average (mean ± SEM) time course of the difference between the 1st and 2nd tuning curve slopes (2nd – 1st) and the significant time points. (C) Grand average (mean ± SEM) time course of the sum of the 1st and 2nd tuning curve slopes (1st + 2nd). (D) Subject-by-subject correlations between the decoding performance and the recency effect were calculated at each time point. Horizontal lines below indicate time points of significant behavioral correlations (Pearson's correlation after multi-comparison correction) for the 1st (blue) and 2nd (red) items, respectively. (E) Left: scatterplot (N = 24) of recency effect vs. 1st decoding strength averaged over t1 (0.67 – 0.72 s after impulse). Right: scatterplot of recency effect vs. 2nd decoding strength averaged over t2 (0.4 – 0.43 s after impulse). (F) Scatterplot (N = 24) of recency effect vs. decoding difference (2nd at T2 – 1st at T1). Each dot represents an individual subject. (Horizontal solid line: cluster-based permutation test, cluster-defining threshold $p < 0.05$, corrected significance level $p < 0.05$; Horizontal dashed line: marginal significance, cluster-defining threshold $p < 0.1$, $0.05 <$ cluster $p < 0.1$).

Reactivation profiles correlate with recency effect (Experiment 1)

We next evaluated the behavioral relevance of the reactivation profiles on a subject-by-subject basis, by relating the decoding strength to the recency effect, a typical behavior in sequence memory, at each time point. As shown in Figure 3D, both the 1st (blue) and 2nd (red) item reactivations significantly correlated with the recency effect (horizontal lines, blue for the 1st item and red for the 2nd item), at different time points (1st item: 0.65 – 0.72 s, corrected cluster p = 0.055, blue shades; 2nd item: 0.4 – 0.5 s, corrected cluster p = 0.038, red shades). Specifically, the recency effect covaried positively with the 2nd item (Figure 3E, right panel; Pearson's correlation, N = 24, r =

0.50, p = 0.013) and negatively with the 1st item (Figure 3E, left panel; Pearson's correlation, N = 24, r = -0.55, p = 0.005). To further confirm the results, we chose the time bins showing significant decoding performance in the previous independent analysis (Figure 3A; T1 for the 1st item, blue shades; T2 for the 2nd item, red shades). Consistently, the 2nd – 1st reactivation difference was correlated with the recency effect (Figure 3F; Pearson's correlation, N = 24, r = 0.47, p = 0.02). Taken together, the backward reactivation profiles that might index distinct latent states in WM, show strong relevance to memory behavior, i.e., stronger recency effect is accompanied by larger, early 2nd item reactivation and weaker, late 1st item reactivation during the delay period.

Experimental procedure and disrupted recency effect (Experiment 2)

One possible reason for the backward reactivation as observed in Experiment 1 is that the 2nd item enters the memory system later than the 1st item and thus decays more slowly, leading to a more excitable state for the lately presented item in the brain. In other words, the distinct latent states might solely arise from their different passive memory traces left in the network. To address the issue, we performed Experiment 2 using the same stimuli and paradigm as Experiment 1, except that subjects did not need to memorize the temporal order of the two orientations. Specifically, as shown in Figure 4A, subjects viewed two serially presented gratings and were instructed to memorize the two orientations. During the recalling period, instead of indicating the 1st or 2nd orientation subjects need to recall as in Experiment 1, a retro-cue appeared to instruct subjects which item that has either smaller or larger angular values (relative to a vertical axis in a clockwise direction) would be tested later. Next, a probe grating was presented and participants indicated whether the orientation of the probe was rotated clockwise or anticlockwise relative to the cued grating. Thus, if the different latent states are due to the passive decay of the serially presented items, we would expect similar recency effect as well as backward reactivation as that in Experiment 1.

Twenty-four subjects participated in Experiment 2. As shown in Figure 4B, interestingly, the 1st and 2nd items showed similar memory performance (1st item: mean = 0.77, s.e. = 0.011; 2nd item: mean = 0.78, s.e = 0.011; paired t-test, df = 23, t = 1.57, p = 0.13, Cohen's d = 0.32). As shown in Figure 4CD, the psychometric

functions did not differ in slopes for the 2nd and 1st orientations (N = 24, 1st item: mean = 0.11, s.e. = 0.008; 2nd item: mean = 0.12, s.e = 0.009; paired t-test, df = 23, t = 1.38, p = 0.18, Cohen's d = 0.28). Thus, recency effect tends to be disrupted when the ordinal structure is not needed to be retained in WM.

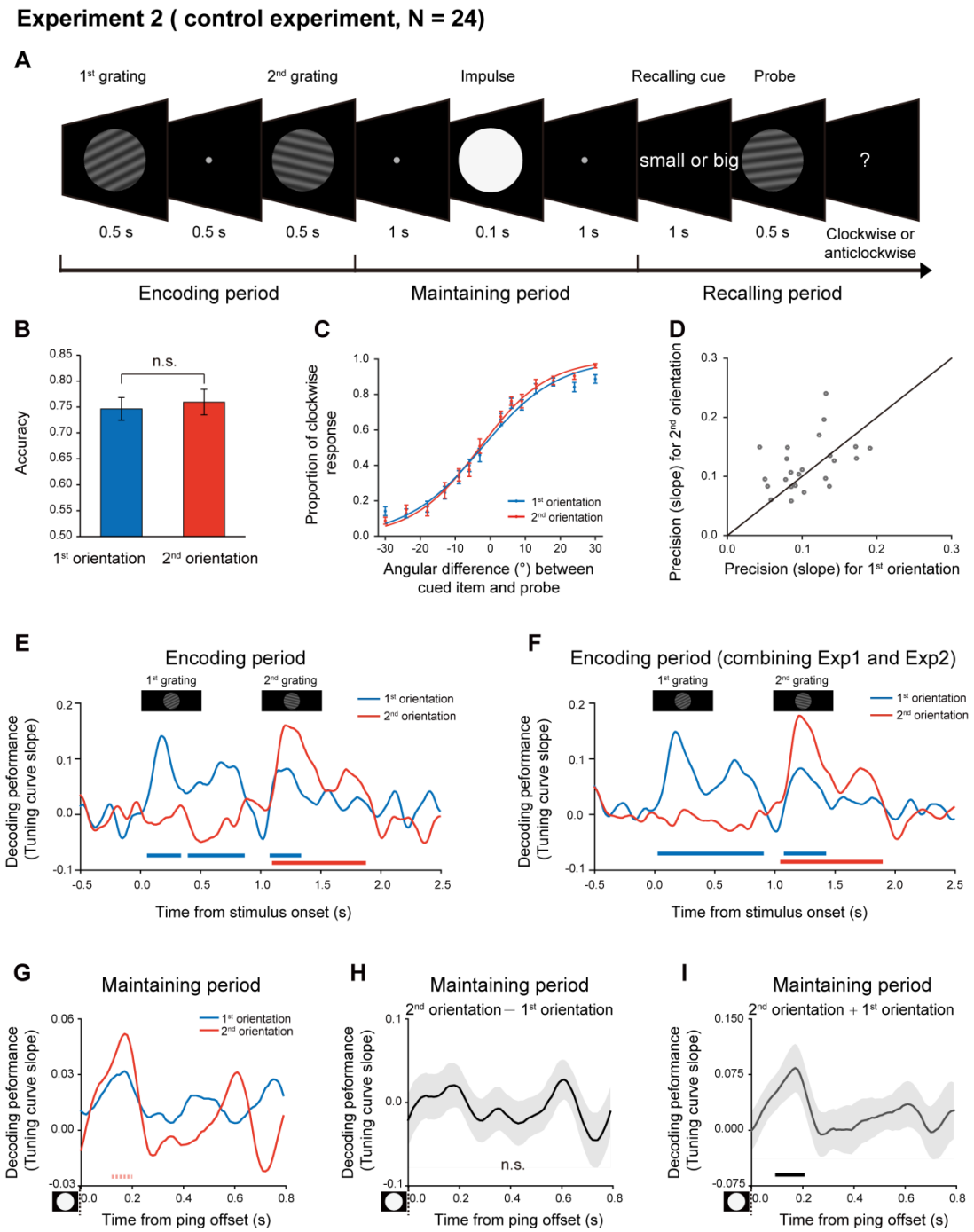

Figure 4: Experimental paradigm and results (Experiment 2). (A) Experiment 2 (N = 24) had the same stimuli and paradigm as Experiment 1, except that subjects did not need to retain the temporal order of the two orientation features. Subjects were first sequentially presented with two

grating stimuli (1st and 2nd gratings) and needed to memorize the two orientations. During the recalling period, a retro-cue (small or big in character) appeared to instruct subjects which item that has either smaller or larger angular values relative to the vertical axis in a clockwise direction would be tested later. Next, a probe grating was presented and participants indicated whether the orientation of the probe was rotated clockwise or anticlockwise relative to that of the cued grating. (B) Grand average (mean ± SEM) behavioral accuracy for the 1st (blue) and 2nd (red) orientations. (C) Grand average (mean ± SEM) psychometric functions for the 1st (blue) and 2nd (red) orientations as a function of the angular difference between the probe and cued orientation. (D) Scatter plot for the slope of the psychometric function for the 1st (x axis) and 2nd (y axis) orientations. (E) Grand average time courses of the tuning curve slopes for the 1st (blue) and 2nd (red) orientations during the encoding period. Horizontal lines below indicate significant time points for the 1st (blue) and 2nd (red) orientations. (F) The same as E, but pooling Experiment 1 and Experiment 2 together during the encoding period (N = 48). (G) Grand average time courses of the tuning curve slope for the 1st (blue) and 2nd (red) WM orientations after the impulse (inset in the bottom left) during retention. (H) Grand average (mean ± SEM) time course of the difference between 1st and 2nd tuning curve slopes (2nd – 1st). (I) Grand average (mean ± SEM) time course of the sum of the 1st and 2nd tuning curve slopes (1st + 2nd) and significant time points. (Horizontal solid line: cluster-based permutation test, cluster-defining threshold $p < 0.05$, corrected significance level $p < 0.05$; Horizontal dashed line: marginal significance, cluster-defining threshold $p < 0.1$, $0.05 <$ cluster $p < 0.1$).

Disrupted backward reactivations during retention (Experiment 2)

We next used the same IEM approach to reconstruct the time-resolved neural representations of orientation features at each time point in Experiment 2. First, the encoding period showed a similar pattern as that of Experiment 1 (Figure 4E). Specifically, the decoding performance of the 1st (blue) and 2nd (red) orientations displayed successive temporal profiles that were time-locked to the presentation of the corresponding grating stimuli (1st item: 0.07 – 0.32 s, corrected cluster $p = 0.005$; 0.41 – 0.85 s, corrected cluster $p = 0.002$; 1.09 – 1.32 s, corrected cluster $p = 0.005$; 2nd item: 1.11– 1.86 s, corrected cluster $p < 0.001$). As shown in Figure 4F, combining Experiment 1 and Experiment 2 revealed a clear serial profile during the encoding period (1st item: 0.04 – 0.89 s, corrected cluster $p < 0.001$; 1.09 – 1.41 s, corrected cluster $p = 0.003$; 2nd item: 1.06 – 1.88 s, corrected cluster $p < 0.001$).

In contrast, the reactivation profiles during the delay period in Experiment 2 did not show the backward pattern as observed in Experiment 1. Instead, as illustrated in Figure 4G, the decoding performance for the 1st and 2nd WM orientations displayed similar temporal courses (0.1 – 0.2 s; 1st item, $p = 0.056$, one-tailed; 2nd item, $p = 0.019$, one-tailed). Consistently, the difference course between the 1st and 2nd decoding performances did not reach any statistical significance (Figure 4H; corrected cluster $p > 0.5$). Meanwhile, as shown in Figure 4I, different from Experiment 1 (Figure 3C), the sum of the 1st and 2nd decoding performance showed significant

responses (0.1 – 0.2 s, corrected cluster p = 0.024), further supporting their common reactivation profiles. In sum, when the two serially presented items are maintained in WM without a sequence structure imposed on them, they tend to be stored in comparable latent states of WM network, thereby having similar probability to be activated after the transient impulse and showing common reactivation profiles. The findings also exclude the possibility that it is the different passive memory decay that gives rise to the different latent states as observed in Experiment 1.

Two-stream Bayesian integration model

We next built a Bayesian integration model (Knill & Pouget, 2004; Ma, 2019) to assess the contribution of two possible factors – low-level passive memory decay and high-level ordinal structure – to the recency effect and reactivation profiles. The rationale of the model is depicted in Figure 5A, i.e., each item is represented in WM via two independent sources: a low-level stream that characterizes its passive representational decay over time (lower) and a high-level stream that signifies the abstract structure in which the item resides (upper). Specifically, for a given item (s) and its representation in low-level (x) and high-level (y) streams, the corresponding likelihood functions ($P(x|s)$, $P(y|s)$) could be modelled as a Gaussian distribution with means and standard deviations as (x, $\sigma_0 + \beta t$) and (y, σ), respectively.

For the low-level stream (x, $\sigma_0 + \beta t$), $\sigma_0 + \beta t$ describes the passive decay of representation precision over time (σ_0: basic memory strength; β: memory decay rate; t: time interval between the item offset and the recalling cue). Since the 1st item appears prior to the 2nd item, it would have a longer t and in turn undergoes larger representational decay compared to the 2nd item, leading to the recency effect. The high-level stream (y, σ), on the other hand, signifies the abstract structure that organizes WM items by assigning different representational precision to items at different positions of a sequence (σ_1 for the 1st item, σ_2 for the 2nd item; lower value indicates higher representation precision).

Notably, both the low-level and high-level streams would contribute to the recency effect, characterized by β and $\sigma_1 - \sigma_2$, respectively. The two streams then converge at the recalling cue and determine the subsequent memory performance. In summary, a Bayesian integration model of five parameters (σ_0, β, σ_1, σ_2, λ) was

established to describe sequence memory behavior, with contributions from both low-level (σ_0 and β) and high-level (σ_1 and σ_2) streams (λ: guessing in decision; see more details in Methods).

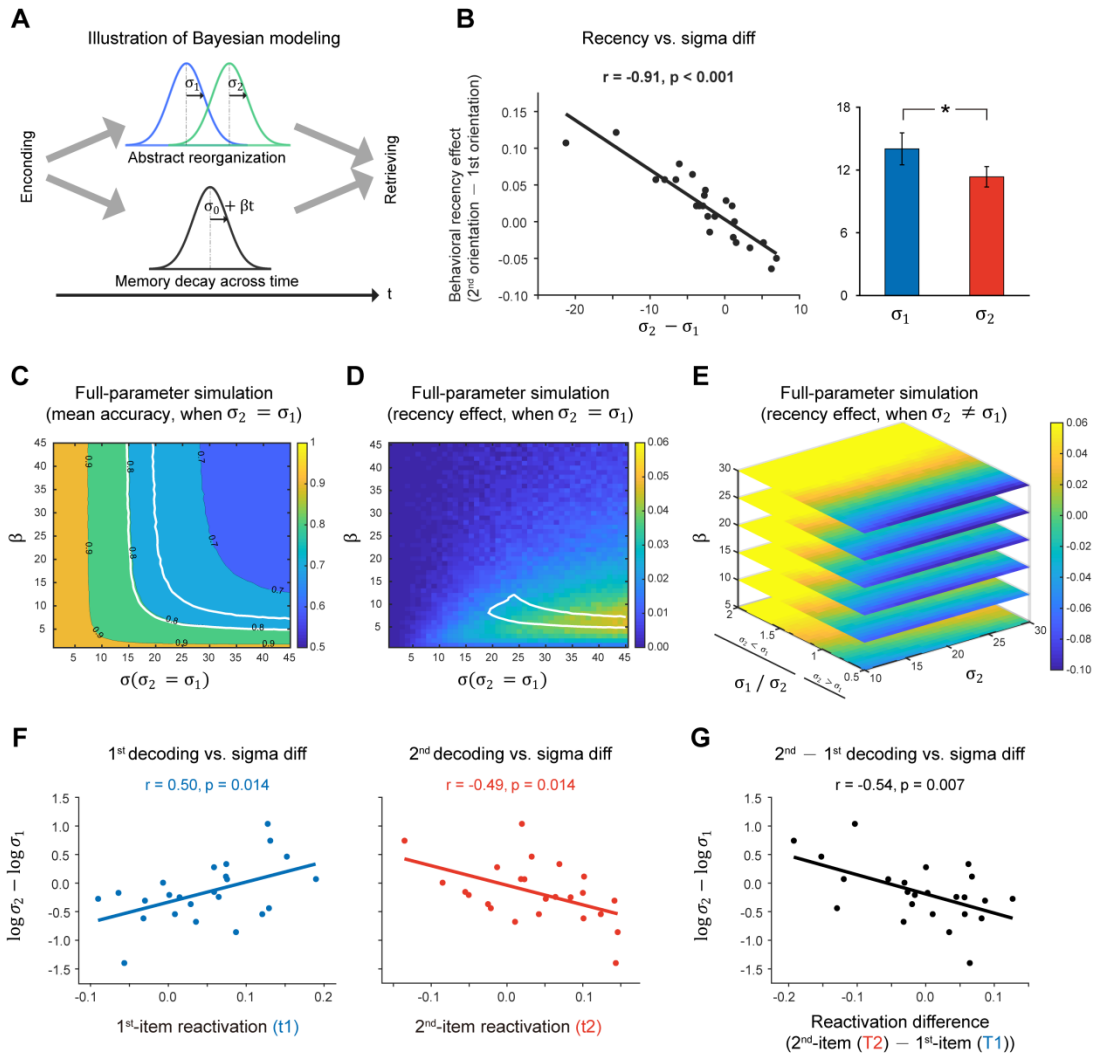

Figure 5: Two-stream Bayesian integration model, full-parameter simulation and relevance to neural reactivations. (A) Illustration of the two-stream Bayesian integration model. Each WM item goes through two streams: one low-level stream that characterizes the passive memory decay over time (lower), one high-level stream that characterizes the abstract ordinal structure (upper). The low-level stream is characterized by a Gaussian distribution with a standard deviation of $\sigma_0 + \beta t$ (σ_0: basic memory strength; β: decay rate; t: time interval between item offset and recalling cue). The high-level stream comprises two Gaussian distributions for the 1st and 2nd items separately, having their respective standard deviations (1st item: σ_1, blue; 2nd item: σ_2, green). (B) Model fitting results. Left panel: Scatterplot (N = 24) of $\sigma_2 - \sigma_1$ vs. behavioral recency effect for Experiment 1. Each dot represents each subject. Right panel: grand average (mean ± SEM) estimated σ_1 and σ_2 in Experiment 1. (*: $p \leq 0.05$). (C-E) Full-parameter simulation results. (C) Simulated averaged memory performance across the 1st and 2nd items as a function of β, σ_1, and σ_2, with $\sigma_2 = \sigma_1$ constraint to eliminate the high-level stream contribution. The region marked by white lines indicates the 95% confidence interval of the empirical memory accuracy in Experiment 1 ([0.76,0.80]). (D) Simulated recency effect as a function of β, σ_1, and

σ_2, with $\sigma_2 = \sigma_1$ constraint. Note that only a small range of parameters could yield the recency effect as well as comparable memory accuracy (area within white lines). (E) Simulated recency effect as a function of β, σ_1 / σ_2, σ_2, without the $\sigma_2 = \sigma_1$ constraint (contributions from both streams). Note the prominent recency effect across a wide range of parameter combinations, independent of low-level stream parameters (β). As expected, larger σ_1 / σ_2 difference corresponds to stronger recency effect. (F-G) Correlation between the estimated high-level modeling parameters and neural reactivations. (F) Scatterplot (N = 24) of ($log\,\sigma_2 - log\,\sigma_1$) vs. 1st decoding strength averaged over t1 (Left) and ($log\,\sigma_2 - log\,\sigma_1$) vs. 2nd decoding strength averaged over t2 (Right). (G) Scatterplot (N = 24) of ($log\,\sigma_2 - log\,\sigma_1$) vs. decoding difference (2nd at T2 – 1st at T1). Each dot represents an individual subject.

Model fitting, full-parameter simulation and relevance to neural reactivations

We next fitted the Bayesian integration model (Figure 5A) to individual data and estimated the parameters for each participant. Interestingly, the recency effect was not correlated with the decay rate β in the low-level stream (Pearson's correlation; N = 24, r = -0.20, p = 0.35), but significantly covaried with $\sigma_2 - \sigma_1$ in the high-level stream (Pearson's correlation; N = 24, r = -0.91, p < 0.001; Figure 5B, left). Furthermore, $\sigma_2 - \sigma_1$ (mean = -2.68, s.e = 1.30) was smaller than 0 (paired t-test, df = 23, t = -2.06, p = 0.05, Cohen's d = 0.42; Figure 5B, right), also consistent with the significant recency effect in Experiment 1. Meanwhile, $\sigma_2 - \sigma_1$ (mean = -1.72, s.e = 1.89) was not different from 0 (paired t-test, df = 23, t = -0.90, p = 0.37, Cohen's d = 0.19) in Experiment 2, also in line with the observed disrupted recency results. Thus, rather than the passive memory decay quantified in the low-level stream (β), the recency effect mainly arises from the representation precision difference ($\sigma_2 - \sigma_1$) retained in the high-level stream that characterizes the abstract ordinal structure of WM items. Moreover and importantly, the high-level representation is also influenced by different task instructions, i.e., showing different σ_1 and σ_2 when ordinal structure is explicitly required to be retained in WM (Experiment 1), while not when the ordinal structure is not task-relevant (Experiment 2).

After fitting the Bayesian integration model to the empirical data, we further ran a full-parameter simulation analysis to attain a better understanding of how the parameters (β, σ_1, σ_2; β, σ_1, $\sigma_2 \in [1,45]$) systematically influence the recency effect. First, we constrained the influence from the high-level stream by defining $\sigma_2 = \sigma_1$ so that the recency effect could only emerge from the low-level accounts. Figure 5C plots the simulated memory performance averaged across the 1st and 2nd items (ranged from 0.5 to 1) as a function of β and σ_1, σ_2 ($\sigma_2 = \sigma_1$) . The area between the white

lines (Figure 5C) delineates the simulated memory accuracy range that is consistent with our empirical results (mean = 0.78; 95% confidence interval, [0.76,0.80]), and Figure 5D plots the corresponding simulated recency effect ($2^{nd} - 1^{st}$) under the same $\sigma_2 = \sigma_1$ constraint. Combining Figure 5C and 5D reveals that only a small range of parameters could yield the recency effect (denoted by white line in Figure 5D), supporting the inefficiency of low-level memory decay in accounting for the recency effect. Next, we removed the high-level constraint by allowing different σ_1 and σ_2. In contrast, as shown in Figure 5E, incorporation of high-level stream contribution ($\sigma_1 \neq \sigma_2$) in the simulation reveals essentially prominent recency effects across a wide range of parameter combinations, largely independent of the low-level stream parameters (β). Moreover, as expected, larger $\sigma_1 - \sigma_2$ difference is associated with stronger recency effect.

Finally, we examined whether the fitted high-level stream parameters ($log\,\sigma_2 - log\,\sigma_1$) were related to the 1st and 2nd item neural reactivations, on a subject-by-subject basis. To this end, we used the time ranges defined in the previous recency-based analysis (Figure 3D, t1 for the 1st item; t2 for the 2nd item). As shown in Figure 5F, $log\,\sigma_2 - log\,\sigma_1$ showed the similar neural relevance as the recency effect (Left panel: 1st item, Pearson's correlation, N = 24, r = 0.50, p = 0.014; Right panel: 2nd item, Pearson's correlation, N = 24, r = -0.49, p = 0.014). Consistently, the $2^{nd} - 1^{st}$ reactivation difference covaried with $log\,\sigma_2 - log\,\sigma_1$ (Figure 5G; Pearson's correlation, N =24, r = -0.54, p = 0.007), when using time bins of significant decoding performance (Figure 3A; T1 for the 1st item, blue shades; T2 for the 2nd item, red shades).

Taken together, the results support the central function of the high-level stream, which represents and maintains the abstract ordinal structure information of to-be-memorized items independent of low-level memory decay, in mediating the sequence memory behavior as well as the latent neural states (i.e., reactivation profiles).

Discussion

In two MEG experiments, we examined how the sequence structure imposed on a list of WM items shapes their neural representations in the human brain. Items located in different positions of a list are stored in distinct latent states of the WM neural network, being reactivated at different latencies. The reactivation pattern correlates with the recency effect in recognition behavior. In contrast, memorizing the same list of items without sequence structure requirements does not elicit the dissociated temporal profiles and displays disrupted recency effect. A dual-stream Bayesian integration model and full-parameter simulations suggest that the ordinal structure of WM items that are characterized in the high-level representations gives rise to the recency effect and further covaries with the reactivation profiles. Taken together, sequence structure, as a form of prior abstract knowledge, essentially modulates memory performance by reorganizing contents into different latent states of the WM neural network.

It has long been posited that WM relies on sustained neuronal firing during the delay period (Curtis & D'Esposito, 2003; Goldman-Rakic, 1995). Meanwhile, recent neural recordings and computational modeling advocate that memory could also be maintained in synapse weights without relying on sustained neural activities (i.e., hidden state), through short-term neural plasticity (STP) principles (Miller et al., 2018; Mongillo et al., 2008; Rose et al., 2016; Sprague et al., 2016; Stokes, 2015; Trübutschek et al., 2017; Wolff et al., 2017). But how can we assess the retained WM information from an activity-silent neural network? Recent studies, by developing an interesting impulse-response approach, show that the neural representation of task-relevant features could be successfully reactivated from the WM network (Wolff et al., 2017, 2020). Furthermore, items associated with different levels of task relevance are found to be retained in different states. For instance, the immediately task-relevant item is in a more excitable state and tends to be first reactivated, whereas the item that is potentially task-relevant in the future resides in an activity-silent state and emerges later. In the current study, the items ordered in a list are equally task-relevant and have the same probability to be tested in the recalling period. Therefore, our findings could not be explained in terms of top-down, task-related attentional modulation as shown before. Instead, our findings provide new evidence supporting that the high-

level abstract knowledge, i.e., sequence structure, arranges items into different latent states in the WM network and influences subsequent memory behavior.

In addition to top-down attentional modulation, low-level features could also modulate the excitability of neural populations. A theoretical model posits that multiple items, located in different excitable states according to their bottom-up saliency levels, would be reactivated at different phases within an alpha-band cycle (Jensen et al., 2012, 2014). Here, given the serial presentation of items during the encoding period, the lately presented item would presumably have less memory decay and in turn higher saliency level, hence residing in a more excitable state. However, two aspects of the results excluded the explanation. First, Experiment 2 used the same sequence of items as Experiment 1, yet did not reveal the temporally dissociated reactivation profiles. Indeed, when the sequence structure is not needed to be retained in WM, the two items are reactivated at similar latencies, indicating that they are stored in comparable latent states to be excited. Second, consistent with the idea, the computational modeling demonstrates that the passive memory decay characterized in the low-level stream could not reliably capture the recency effect; rather, it is the sequence structure embedded in the high-level stream that plays a central function in modulating recency effect and correlates with neural reactivation profiles.

Structure information has long been viewed to influence perception and memory, e.g., global precedence effect (Chen, 1982; Navon, 1977), reverse hierarchy theory (Ahissar & Hochstein, 2004), etc. Recently, it has been suggested that structural information and content information can be encoded in a separate and independent manner to facilitate generalization (Behrens et al., 2018; Bengio et al., 2013; Higgins et al., 2017). Memory performance also tends to be influenced by the contexts the items are embedded in (DuBrow & Davachi, 2013; Gershman et al., 2013), and when two items belong to different contexts, the memory performance for their temporal order relationship would be largely disrupted. Furthermore, in a pure-tone frequency auditory discrimination task, subjects show a tendency to hold a perceptual anchor throughout the experiment, also signifying the influence of structure information (i.e., a statistical map across all stimuli) on local perception (Harris, 1952; Mathias et al., 2020). Most relevantly, one study shows that when performing a two-line orientation WM task, human subjects display a strong impact from the relative relationship

between the two lines on the individual memory behavioral performance (Ding et al., 2017). In other words, the abstract structure that characterizes the relationship between WM items spontaneously reshapes the representation of each item in WM. Here, in line with previous findings, our results provide new converging behavioral, neural, and computational modeling evidence advocating the strong influence of high-level sequence structure on WM behavior and the underlying neural implementations – reorganization of items into different latent states.

The backward reactivation profile suggests that items located in the late position of a sequence are stored in a more excitable state, compared to those in the early position. The results are well consistent with our previous findings, whereby a temporal response function (TRF) approach was employed to tag the neural reactivations during retention when subjects perform a sequence memory task. In that study, we also observed a backward reactivation profile, i.e., shorter latency for recent versus early items, which is also related to the recency effect (Huang et al., 2018). Meanwhile, the current findings differ from previous results in important ways. Specifically, the TRF latency refers to a relative time basis, whereas the present design assessed neural representations in absolute time after the impulse stimulus, thus constituting new evidence for the backward reactivation. Moreover, the computational modeling as well as the control experiment further advocates that it is the high-level structure rather than the passive memory decay that mainly accounts for the recency effect and backward reactivations, an unresolved issue in the previous study (Huang et al., 2018). In fact, backward reactivations have been observed in many situations, e.g., during break after spatial experience in rats (Foster & Wilson, 2006), performing a reasoning task in humans (Kurth-nelson et al., 2016), etc. Interestingly, a recent study shows that during structure learning, a forward replay during resting would reverse in direction when paired with reward (Liu et al., 2019), implying the involvement of reinforcement learning principles (Schultz et al., 1997; Sutton & Barto, 1998). Taken together, a possible interpretation for the backward reactivation is that the item located in the late position of a list might serve as an anchoring point in memory for other WM items and is in turn maintained in a more excitable latent state, given that the recent item receives less inference and carries more reliable information for memory retrieval.

We built a two-stream Bayesian integration model (Knill & Pouget, 2004; Ma, 2019) that incorporates both low-level memory decay and high-level abstract structure. Although both streams could in principle contribute to the recency effect, the model fitting and full-parameter simulations confirm that it is the high-level sequence knowledge rather than the low-level passive decay that mostly accounts for the recency effect. This is consistent with a previous study combining behavioral measurements and computational modeling, revealing that low-level, absolute judgments fail to account for high-level, relative judgements (Ding et al., 2017). Furthermore, the high-level representations could also be modulated by task instructions, also in agreement with views that multiple items are prioritized according to either reward or other factors in WM (Allen & Ueno, 2018; Atkinson et al., 2018; Hu et al., 2014; Makovski & Jiang, 2007; Thomas et al., 2016). It is noteworthy that our findings largely differ from the typical top-down attentional modulation results (Rose et al., 2016; Sprague et al., 2016; Wolff et al., 2017; Yu & Postle, 2018), given that all the items are equally task-relevant in both Experiment 1 and Experiment 2. Instead, it is the sequence structure knowledge that prioritizes the representation of the recent item in the high-level stream. Finally, in addition to behavioral evidence and modeling results, our MEG results further reveal how the abstract sequence structure signified in the high-level stream of the computational model is implemented in the human brain, that is, reorganizing WM items into different latent states of WM neural network.

Author contributions

Q.H. and H.L. designed the experiment. Q.H. performed MEG experiments and data analysis. H.Z. built the model. Q.H, H.Z., and H.L. wrote the paper.

Competing interests

The authors declare no competing interests.

Acknowledgments

We thank Dr. Qing Yu and Dr. Ce Mo for helpful comments. This work was supported by the National Natural Science Foundation of China (31930052 to H.L.),

and Beijing Municipal Science & Technology Commission (Z181100001518002 to H.L.). We also thank the National Center for Protein Sciences at Peking University for assistance with MEG experiments. Dr. Huihui Zhang was supported by Peking University Boya Postdoctoral Fellowship.

Materials and Methods

Ethics statement

Written informed consent was provided by all participants. Experimental protocols were approved by the Research Ethics Committee of Peking University and adhered to the principles conveyed in the Declaration of Helsinki.

Participants

Twenty-four subjects (15 males, 21 ± 1.8 years old) participated in Experiment 1, and another 24 subjects (15 males, 21 ± 1.7 years old) participated in Experiment 2. All subjects had normal or corrected-to-normal vision, with no history of psychiatric or neurological disorders. All subjects provided informed consent prior to the start of the experiment.

Stimuli and tasks

Experiment 1: each trial consisted of three phases – encoding, maintaining, and recalling. During the encoding period, participants were presented with two 0.5 s gratings (6° × 6°) sequentially at the center (0.5 s interval between them), and were instructed to memorize the orientations of the two gratings as well as their order, i.e., the 1st orientation, the 2nd orientation. For each trial, the orientations of the gratings were drawn from a uniform distribution over 25°– 175° in 25° increments, plus a small random angular jitter (± 1° – ± 3°). During the maintaining period, after 1 sec, a high luminance disc (30 cd/m^2) appeared at the center for 0.1s, followed by another 1 s interval. During the recalling period, a retrospective cue (‘1’ or ‘2’ character) was first presented for 1 s to instruct subjects either the 1st or 2nd orientation would be tested. A probe grating (6° × 6°) was then presented for 0.5 sec at the center and participants indicated whether the orientation of the probe was rotated clockwise or anticlockwise relative to that of the cued grating. The angular differences between a memory item and the corresponding memory probe were uniformly distributed across seven angle differences (± 3°, ± 6°, ± 9°, ± 13°, ± 18 °, ± 24°, ± 30°). During each trial, all participants were instructed to keep the number of eye blinks to be minimum. Participants should complete 280 trials in total, which took approximately 40 min (including breaks).

Experiment 2: Experiment 2 had the same stimuli and paradigm as Experiment 1, except that subjects did not need to retain the temporal order of the two orientation features. Specifically, in each trial, subjects were first sequentially presented with two grating stimuli and needed to memorize the two orientations without needing to retain their temporal order as in Experiment 1. During the maintaining period, a high luminance disc that did not contain any orientation information was presented. During the recalling period, a retro-cue appeared to instruct subjects which item that has either smaller or larger angular values relative to the vertical axis in a clockwise direction ('big' or 'small' in character) would be tested later. Next, a probe grating was presented and participants indicated whether the orientation of the probe was rotated clockwise or anticlockwise relative to that of the cued grating.

Participants completed the MEG inside a sound-attenuated, dimly lit, and magnetically shielded room. Stimuli were displayed onto a rear-projection screen (placed at a viewing distance of 75 cm) with a spatial resolution of 800 × 600 pixels and a refresh rate of 60 Hz.

MEG recordings and preprocessing

Neuromagnetic data were acquired using a 306-sensor MEG system (204 planar gradiometers, 102 magnetometers, Elekta Neuromag system, Helsinki, Finland) at Peking University, Beijing, China. Head movements across sessions should be within 3 mm for data to be involved for further analysis. The spatiotemporal signal space separation (tSSS) was used to remove the external noise (Taulu & Simola, 2006). Furthermore, both horizontal and vertical electrooculograms (EOGs) were recorded. MEG data were recorded at 1000 Hz sampling frequency. The MEG data was preprocessed offline using FieldTrip software (Oostenveld et al., 2011). Specifically, the data was offline band-pass filtered between 2 and 30 Hz. Independent component analysis was then performed in each subject to remove eye-movement and artifact components, and the remaining components were then back-projected to channel space. All data was then downsampled to 100 Hz. Trials with large variances or contained excessive or irregular artifacts were manually removed. Since here we focused on the orientation representations in the MEG response, only posterior MEG channels, including parietal sensors (52 planar gradiometers, 26 magnetometers) and

occipital sensors (48 planar gradiometers, 24 magnetometers), were used for further analysis.

Data analysis

Behavioral performance analysis

In addition to overall behavioral accuracy estimation, to further assess the psychometric function for orientation memory performance, we quantified the response proportion as a function of the angular difference between WM orientation and probe orientation. This function was further fitted in each subject, by $y = 1/(1 + e^{(-\beta*(x-\mu))})$, where β represents the slope and μ is the bias parameter. The estimated slope β could represent memory precision, with larger value corresponding to better memory performance.

Time-resolved orientation decoding

To assess the time-resolved orientation information from the MEG signals, we used an inverted encoding model to reconstruct the orientation tuning of the grating stimulus from the neural activities at each time point. This method has been previously used on many features, such as color (Brouwer & Heeger, 2009), orientation (Brouwer & Heeger, 2011; Ester et al., 2015; Kok et al., 2017; Myers et al., 2015), and spatial location (Sprague et al., 2014, 2016; Sutterer et al., 2019). One assumption of the model is that the response in each sensor could be approximated as a linear sum of underlying neural populations encoding different values of the feature-of-interest (e.g., orientation) separately, and therefore, by grouping the contributions from many sensors, we could achieve an estimation of the underlying neural population responses.

We began by modelling the response of each MEG sensor as a linear sum of seven information channels. B_1 (m sensors × n trials) represents the observed response at each sensor for each trial in the training set. C_1 (k channels × n trials) represents the predicted responses of each of the k information channels (i.e., k = 7 here) that are determined by basis functions, for each trial. W (m sensors × k channels) represents the weight matrix that characterizes the linear mapping from 'channel space' to

‘sensor space’. Taken together, their relationship could be described by a general linear model $B_1 = WC_1$.

Specifically, similar to previous studies (Brouwer & Heeger, 2011; Ester et al., 2015), the basis functions that would determine C_1 are designed to contain seven half-wave rectified sinusoids centered at different orientation values (25°, 50°, 75°, and so on) and raised to the 6th power. The weight matrix W (m sensors × k channels) could thus be estimated via using least-squares regression $\widehat{W} = B_1 C_1^T (C_1 C_1^T)^{-1}$.

After establishing W that links sensor space to the underlying information channels responses from the training set, we then used the estimated $\widehat{W}$ to test on independent datasets B_2 (sensors × trials) and calculated the predicted responses of the seven information channels, by $\hat{C}_2 = (\widehat{W}^T \widehat{W})^{-1} \widehat{W}^T B_2$.

The estimated channel responses $\hat{C}_2$ was then circularly shifted to a common center (0°) in reference to the orientation-of-interest in each trial, which were further averaged across trials. A leave-one-out cross-validation was implemented such that data from all but one experimental block was used as B_1 to estimate $\widehat{W}$, while data from the remaining block was used as B_2 to estimate $\hat{C}_2$, to ensure the independence between training set and testing set. The entire analysis was repeated on all combinations, and the resulting information channel responses were then averaged. Note that the procedure was performed at each time point so a time-resolved tuning curve for each subject was obtained.

To further characterize the orientation decoding performance, the slope of the calculated channel responses (tuning curve) at each time was estimated using linear regression. The slope time courses were further smoothed with a 40 ms Gaussian kernel. The time-resolved decoding performance was tested by using one-sample t-test on the estimated slope against zero followed by multiple comparison correction across time (FieldTrip, cluster-based permutation test, 1000 permutations) (Maris & Oostenveld, 2007). All statistical tests were two-sided unless stated otherwise.

Correlations between recency behavior and neural reactivation profiles

To evaluate the behavioral relevance of neural reactivation profiles, we computed the Pearson’s correlation between the decoding performance and behavioral recency effect, at each time point, on a subject-by-subject basis. A multiple comparison

correction across time was then performed on the correlation results by using cluster-based permutation test (N = 1000). To further illustrate the subject-by-subject correlations between the decoding strength and recency effect (Figure 3E), we averaged the decoding strengths over time-of-interests for the 1st (t1: 0.67– 0.72 s, after impulse stimulus) and 2nd (t2: 0.4 – 0.43 s, after impulse stimulus) items, respectively, in each subject. The time-of-interests (i.e., t1, t2) were time points showing significant behavioral relevance as well as decoding strength. Note that the time-of-interests were just used for illustration purposes and the correlations between reactivations and the recency effect were independently tested with multiple-comparison correction over time, as described previously (Figure 3D).

We used another criterion to choose time-of-interests based on the decoding strength analysis (Figure 3A), i.e., T1 for the 1st item (0.67 – 0.76 s, after impulse stimulus) and T2 for the 2nd item (0.26 – 0.43 s, after impulse stimulus). The decoding strengths for the 1st and 2nd items were then averaged over T1 and T2, respectively, in each subject. The 2nd – 1st reactivation strength was then correlated with the recency effect (Pearson's correlation; Figure 3F).

The same Pearson's correlation analysis was performed between the high-level modeling parameters $log\,\sigma_2 - log\,\sigma_1$ and decoding strengths (Figure 5FG). Note that the time-of-interests (i.e., t1, t2, T1, T2) were selected based on previous neuro-recency relationship analysis (Figure 3).

Computational modeling and full-parameter simulation

Two-stream Bayesian integration model

We built a computational model to account for the observed recency effect in the framework of Bayesian inference. The model consists of two streams, a low-level stream and a high-level stream, which characterize passive memory decay over time and abstract sequence structure, respectively (Figure 5A).

In the low-level stream, for a given stimulus s (the 1st or the 2nd orientations), the probability distribution of the representation of that orientation x, was assumed to be Gaussian, with precision (standard deviation) decreasing over time. From participants'

perspective, they have an internal representation x, but they do not know s, and the likelihood function of s, $p(x|s)$ could be written as:

$$p(x|s) = \frac{1}{\sqrt{2\pi(\sigma_0+\beta t)^2}} e^{-\frac{(s-x)^2}{2(\sigma_0+\beta t)^2}} \quad (1)$$

Here, β is the decay rate over time and t is the time passed after the stimulus offset. In the current study, at the time of recalling, t = 3.1 s for the 1st orientation, and t = 2.1 s for the 2nd orientation.

In parallel, the 1st and 2nd orientations are also represented in the high-level stream after both of them enter the system. Specifically, for a given stimulus s, the distribution of the representation y was also assumed to be Gaussian, and the likelihood function $p(y|s)$ is centered at y with a standard deviation σ ($\sigma = \sigma_1$ for the 1st orientation, and $\sigma = \sigma_2$ for the 2nd orientation), written as:

$$p(y|s) = \frac{1}{\sqrt{2\pi\sigma^2}} e^{-\frac{(s-y)^2}{2\sigma^2}} \quad (2)$$

The representation precision may also decrease over time, but because the difference between σ_1 and σ_2 remains same over time (same decay rate and decay time), we only used one parameter σ, which represents the standard deviation at the recalling time.

As below, we used one example when recalling the 1st orientation ($\sigma = \sigma_1$) to elucidate how information from the two independent streams are integrated and determine the memory recognition performance in retrieval. According to Bayes' rule, the posterior $p(s|x,y)$ is calculated as below (the prior $p(s)$ was assumed to be constant):

$$p(s|x,y) = \frac{p(x|s)\cdot p(y|s)\cdot p(s)}{\int p(x|s)\cdot p(y|s)\cdot p(s)ds} = \frac{1}{\sqrt{2\pi{\sigma_{int}}^2}} e^{-\frac{(s-u)^2}{2{\sigma_{int}}^2}} \quad (3)$$

The resulted $p(s|x,y)$ is a Gaussian distribution with mean, $u = \frac{y(\sigma_0+\beta t)^2+x{\sigma_1}^2}{{\sigma_1}^2+(\sigma_0+\beta t)^2}$ and variance, ${\sigma_{int}}^2 = \frac{{\sigma_1}^2(\sigma_0+\beta t)^2}{{\sigma_1}^2+(\sigma_0+\beta t)^2}$.

For a given stimulus s_1 across many trials, the conditional probability of retrieved orientation s is a Gaussian distribution centered at s_1 with a standard deviation of σ_s ($\sigma_s{}^2 = \sigma_{int}{}^2 = \frac{\sigma_1{}^2(\sigma_0+\beta t)^2}{\sigma_1{}^2+(\sigma_0+\beta t)^2}$).

To simplify the calculation, we used relative orientations, i.e., s_1 and s_2 were set to 0, and the probe orientation is the relative orientation to the recalled orientation (s_1 or s_2). Thus, on each trial, for a given probe s_p (relative orientation), the conditional probability of response r (r = 1 correct, r = -1, incorrect), $p(r|s_p)$ is given by

$$p(r|s_p) = \begin{cases} \int_{-\infty}^{s_p} \frac{1}{\sqrt{2\pi\sigma_s{}^2}} e^{-\frac{s^2}{2\sigma_s{}^2}} ds, rs_p \geq 0 \\ \int_{s_p}^{\infty} \frac{1}{\sqrt{2\pi\sigma_s{}^2}} e^{-\frac{s^2}{2\sigma_s{}^2}} ds, rs_p < 0 \end{cases} \quad (4)$$

To account for participants' guessing behavior when comparing the probe orientation with the recalled orientation, a parameter λ was included. The conditional probability $p(r|s_p)$ in equation (4) is updated as:

$$p(r|s_p) = \lambda p(r|s_p) + (1-\lambda) \times 0.5 \quad (5)$$

Assuming all trials are independent, the joint probability across all N trials can be written as:

$$p(r^1|s_p^1)p(r^2|s_p^2)p(r^3|s_p^3),\ldots,p(r^N|s_p^N) = \prod_{i=1}^{N} p(r^i|s_p^i) \quad (6)$$

We next changed products to sums by taking the logarithm of both sides.

$$log(p(r^1|s_p^1)p(r^2|s_p^2)p(r^3|s_p^3),\ldots,p(r^N|s_p^N)) = \sum_{i=1}^{N} log(p(r^i|s_p^i)) \quad (7)$$

Together, we built a Bayesian model of five parameters, σ_0, β, σ_1, σ_2, λ to quantify the working memory of each item in a sequence. Here, σ_0 and β belong to the low-level stream, signifying the automatic memory decay with β representing the decay rate. Parameters σ_1 and σ_2 belong to the high-level stream, indicating the representation precisions for the two items assigned by the abstract sequence structure.

Model fitting and full-parameter simulation

The above model was then fitted to individual behavioral data. The five parameters were estimated to produce the largest value of equation (7) with Matlab built-in function fmincon (σ_0, β , σ_1, $\sigma_2 \in [0.1,45]$; $\lambda \in [0,1]$, and $\sigma_1 < \sigma_0 + \beta t_1,\ \sigma_2 < \sigma_0 + \beta t_2$), in each subject, respectively.

We also ran a full-parameter simulation analysis to examine how the memory performance for the 1st and 2nd items would vary with different parameters. The parameter σ_0 was fixed to 3 and the parameter λ was fixed to 1 because they do not contribute to the recency effect. For one set of parameters (candidate parameters), we sampled 24 observers using the same trials in experiment 1 to simulate the responses. For each simulated observer, the parameters were sampled from a Gaussian distribution centered at the candidate parameters with a standard deviation of 20% percent of the candidate parameters. The group average was then calculated. To improve simulation stability, the procedure was repeated 100 times.

Reference

Ahissar, M., & Hochstein, S. (2004). The reverse hierarchy theory of visual perceptual learning. *Trends in Cognitive Sciences*, *8*(10), 457–464.

Baddeley, A. (2003). Working memory: Looking back and looking forward. *Nature Reviews Neuroscience*. https://doi.org/10.1038/nrn1201

Bae, G. Y., Olkkonen, M., Allred, S. R., & Flombaum, J. I. (2015). Why some colors appear more memorable than others : a model combining categories and particulars in color working memory. *Journal of Experimental Psychology General*, *144*(4), 744.

Behrens, T. E. J., Muller, T. H., Whittington, J. C. R., Mark, S., Baram, A. B., Stachenfeld, K. L., & Kurth-nelson, Z. (2018). What Is a Cognitive Map ? Organizing Knowledge for Flexible Behavior. *Neuron*, *100*(2), 490–509. https://doi.org/10.1016/j.neuron.2018.10.002

Bengio, Y., Mesnil, G., Dauphin, Y., & Rifai, S. (2013). Better mixing via deep representations. *International Conference on Machine Learning*, 552–560.

Brady, T. F., & Alvarez, G. A. (2011). Hierarchical Encoding in Visual Working Memory: Ensemble Statistics Bias Memory for Individual Items. *Psychological Science*, *22*(3), 384–392. https://doi.org/10.1177/0956797610397956

Broadbent, D. E., & Broadbent, M. H. P. (1981). Recency effects in visual memory. *The Quarterly Journal of Experimental Psychology Section A*, *33*(1), 1–15. https://doi.org/10.1080/14640748108400762

Brouwer, G. J., & Heeger, D. J. (2009). Decoding and reconstructing color from responses in human visual cortex. *Journal of Neuroscience*, *29*(44), 13992–14003. https://doi.org/10.1523/JNEUROSCI.3577-09.2009

Brouwer, G. J., & Heeger, D. J. (2011). Cross-orientation suppression in human visual cortex. *Journal of Neurophysiology*, *106*(5), 2108–2119. https://doi.org/10.1152/jn.00540.2011

Chen, L. (1982). Topological structure in visual perception. *Science*, *218*(4573), 699–700.

Curtis, C. E., & D'Esposito, M. (2003). Persistent activity in the prefrontal cortex during working memory. *Trends in Cognitive Sciences*, *7*(9), 415–423. https://doi.org/10.1016/s1364-6613(03)00197-9

Ding, S., Cueva, C. J., Tsodyks, M., & Qian, N. (2017). Visual perception as retrospective Bayesian decoding from high- to low-level features. *Proceedings of the National Academy of Sciences of the United States of America*, *114*(43), E9115–E9124. https://doi.org/10.1073/pnas.1706906114

DuBrow, S., & Davachi, L. (2013). The influence of context boundaries on memory for the sequential order of events. *Journal of Experimental Psychology: General*, *142*(4), 1277.

Ester, E. F., Sprague, T. C., & Serences, J. T. (2015). Parietal and Frontal Cortex Encode Stimulus-Specific Mnemonic Representations during Visual Working Memory. *Neuron*, *87*(4), 893–905. https://doi.org/10.1016/j.neuron.2015.07.013

Foster, D. J., & Wilson, M. A. (2006). Reverse replay of behavioural sequences in hippocampal place cells during the awake state. *Nature*, *440*(7084), 680–683.

Gershman, S. J., Schapiro, A. C., Hupbach, A., & Norman, K. A. (2013). Neural Context Reinstatement Predicts Memory Misattribution. *The Journal of Neuroscience*, *33*(20), 8590 LP – 8595. https://doi.org/10.1523/JNEUROSCI.0096-13.2013

Goldman-Rakic, P. S. (1995). Cellular basis of working memory. *Neuron*, *14*(3), 477–485. https://doi.org/10.1016/0896-6273(95)90304-6
Harris, J. D. (1952). The decline of pitch discrimination with time. *Journal of Experimental Psychology*, *43*(2), 96.
Higgins, I., Matthey, L., Pal, A., Burgess, C., Glorot, X., Botvinick, M., Mohamed, S., & Lerchner, A. (2017). beta-VAE: Learning Basic Visual Concepts with a Constrained Variational Framework. *Iclr*, *2*(5), 6.
Huang, Q., Jia, J., Han, Q., & Luo, H. (2018). Fast-backward replay of sequentially memorized items in humans. *ELife*, *7*, 1–21. https://doi.org/10.7554/eLife.35164
Jensen, O., Bonnefond, M., & VanRullen, R. (2012). An oscillatory mechanism for prioritizing salient unattended stimuli. *Trends in Cognitive Sciences*, *16*(4), 200–206.
Jensen, O., Gips, B., Bergmann, T. O., & Bonnefond, M. (2014). Temporal coding organized by coupled alpha and gamma oscillations prioritize visual processing. *Trends in Neurosciences*, *37*(7), 357–369.
Knill, D. C., & Pouget, A. (2004). The Bayesian brain: the role of uncertainty in neural coding and computation. *TRENDS in Neurosciences*, *27*(12), 712–719.
Kok, P., Mostert, P., & De Lange, F. P. (2017). Prior expectations induce prestimulus sensory templates. *Proceedings of the National Academy of Sciences*, *114*(39), 10473–10478.
Kurth-nelson, Z., Economides, M., Dolan, R. J., Dayan, P., Kurth-nelson, Z., Economides, M., Dolan, R. J., & Dayan, P. (2016). Fast Sequences of Non-spatial State Representations in Humans Article Fast Sequences of Non-spatial State Representations in Humans. *Neuron*, *91*(1), 194–204. https://doi.org/10.1016/j.neuron.2016.05.028
Liu, Y., Dolan, R. J., Kurth-Nelson, Z., & Behrens, T. E. J. (2019). Human Replay Spontaneously Reorganizes Experience. *Cell*, *178*(3), 640-652.e14. https://doi.org/10.1016/j.cell.2019.06.012
Ma, W. J. (2019). Bayesian Decision Models: A Primer. *Neuron*, *104*(1), 164–175.
Maris, E., & Oostenveld, R. (2007). Nonparametric statistical testing of EEG-and MEG-data. *Journal of Neuroscience Methods*, *164*(1), 177–190.
Mathias, S. R., Varghese, L., Micheyl, C., & Shinn-Cunningham, B. G. (2020). On the utility of perceptual anchors during pure-tone frequency discrimination. *The Journal of the Acoustical Society of America*, *147*(1), 371–380. https://doi.org/10.1121/10.0000584
Miller, E. K., Lundqvist, M., & Bastos, A. M. (2018). Working Memory 2.0. In *Neuron*. https://doi.org/10.1016/j.neuron.2018.09.023
Mongillo, G., Barak, O., & Tsodyks, M. (2008). Synaptic theory of working memory. *Science*, *319*(5869), 1543–1546.
Myers, N. E., Rohenkohl, G., Wyart, V., Woolrich, M. W., Nobre, A. C., & Stokes, M. G. (2015). Testing sensory evidence against mnemonic templates. *ELife*, 1–25. https://doi.org/10.7554/eLife.09000
Navon, D. (1977). Forest before trees: The precedence of global features in visual perception. *Cognitive Psychology*, *9*(3), 353–383.
Oostenveld, R., Fries, P., Maris, E., & Schoffelen, J.-M. (2011). FieldTrip: open source software for advanced analysis of MEG, EEG, and invasive electrophysiological data. *Computational Intelligence and Neuroscience*, *2011*.
Rose, N. S., Larocque, J. J., Riggall, A. C., Gosseries, O., Starrett, M. J., Meyering, E.

E., & Postle, B. R. (2016). Reactivation of latent working memories with transcranial magnetic stimulation. *Science*, *354*(6316), 1136–1140.
Schultz, W., Dayan, P., & Montague, P. R. (1997). A neural substrate of prediction and reward. *Science*, *275*(5306), 1593–1599.
Sprague, T. C., Ester, E. F., & Serences, J. T. (2014). Reconstructions of information in visual spatial working memory degrade with memory load. *Current Biology*, *24*(18), 2174–2180.
Sprague, T. C., Ester, E. F., & Serences, J. T. (2016). Restoring Latent Visual Working Memory Representations in Human Cortex. *Neuron*, *91*(3), 694–707. https://doi.org/10.1016/j.neuron.2016.07.006
Stokes, M. G. (2015). "Activity-silent" working memory in prefrontal cortex: A dynamic coding framework. *Trends in Cognitive Sciences*, *19*(7), 394–405. https://doi.org/10.1016/j.tics.2015.05.004
Sutterer, D. W., Foster, J. J., Adam, K. C. S., Vogel, E. K., & Awh, E. (2019). Item-specific delay activity demonstrates concurrent storage of multiple active neural representations in working memory. *PLoS Biology*, *17*(4), 1–25. https://doi.org/10.1371/journal.pbio.3000239
Sutton, R. S., & Barto, A. G. (1998). *Introduction to reinforcement learning* (Vol. 135). MIT press Cambridge.
Taulu, S., & Simola, J. (2006). Spatiotemporal signal space separation method for rejecting nearby interference in MEG measurements. *Physics in Medicine & Biology*, *51*(7), 1759.
Trübutschek, D., Marti, S., Ojeda, A., King, J. R., Mi, Y., Tsodyks, M., & Dehaene, S. (2017). A theory of working memory without consciousness or sustained activity. *ELife*, *6*, 1–29. https://doi.org/10.7554/eLife.23871
Wolff, M. J., Jochim, J., Akyürek, E. G., Buschman, T. J., & Stokes, M. G. (2020). Drifting codes within a stable coding scheme for working memory. *PLoS Biology*, *18*(3), e3000625.
Wolff, M. J., Jochim, J., Akyürek, E. G., & Stokes, M. G. (2017). Dynamic hidden states underlying working-memory-guided behavior. *Nature Neuroscience*, *20*(6), 864–871. https://doi.org/10.1038/nn.4546
Yu, Q., & Postle, B. R. (2018). Different states of priority recruit different neural codes in visual working memory. *BioRxiv*, 334920. https://doi.org/10.1101/334920